Biochemical and Biophysical Research Communications 446 (2014) 399–403

Contents lists available at ScienceDirect

Biochemical and Biophysical Research Communications

journal homepage: www.elsevier.com/locate/ybbrc

Structural insights into PDZ-mediated interaction of NHERF2 and LPA_2, a cellular event implicated in CFTR channel regulation

Joshua Holcomb [a], Yuanyuan Jiang [a], Guorong Lu [a], Laura Trescott [a], Joseph Brunzelle [b], Nualpun Sirinupong [c], Chunying Li [a], Anjaparavanda P. Naren [d,*], Zhe Yang [a,*]

[a] Department of Biochemistry and Molecular Biology, Wayne State University School of Medicine, Detroit, MI, USA
[b] Advanced Photon Source, Argonne National Lab, Argonne, IL, USA
[c] Nutraceuticals and Functional Food Research and Development Center, Prince of Songkla University, Hat-Yai, Songkhla, Thailand
[d] Department of Pediatrics, Cincinnati Children's Hospital Medical Center, Cincinnati, OH, USA

ARTICLE INFO

Article history:
Received 25 February 2014
Available online 12 March 2014

Keywords:
NHERF2
LPA_2
X-ray crystallography
CFTR
Scaffold protein
Cystic fibrosis

ABSTRACT

The formation of CFTR–NHERF2–LPA_2 macromolecular complex in airway epithelia regulates CFTR channel function and plays an important role in compartmentalized cAMP signaling. We previously have shown that disruption of the PDZ-mediated NHERF2–LPA_2 interaction abolishes the LPA inhibitory effect and augments CFTR Cl^- channel activity in vitro and in vivo. Here we report the first crystal structure of the NHERF2 PDZ1 domain in complex with the C-terminal LPA_2 sequence. The structure reveals that the PDZ1–LPA_2 binding specificity is achieved by numerous hydrogen bonds and hydrophobic contacts with the last four LPA_2 residues contributing to specific interactions. Comparison of the PDZ1–LPA_2 structure to the structure of PDZ1 in complex with a different peptide provides insights into the diverse nature of PDZ1 substrate recognition and suggests that the conformational flexibility in the ligand binding pocket is involved in determining the broad substrate specificity of PDZ1. In addition, the structure reveals a small surface pocket adjacent to the ligand-binding site, which may have therapeutic implications. This study provides an understanding of the structural basis for the PDZ-mediated NHERF2–LPA_2 interaction that could prove valuable in selective drug design against CFTR-related human diseases.

© 2014 Elsevier Inc. All rights reserved.

1. Introduction

Cystic fibrosis transmembrane conductance regulator (CFTR) is a cAMP-regulated chloride (Cl^-) channel primarily localized at the apical surfaces of epithelial cells lining the airway, gut and exocrine glands [1,2]. CFTR is responsible for transepithelial salt and water transport and plays critical roles in maintaining fluid homoeostasis, airway fluid clearance, and airway submucosal glands secretion in both healthy and disease phenotypes [3,4]. Growing evidence suggests that CFTR interacts directly or indirectly with other ion channels, transporters, scaffolding proteins, protein kinases, effectors, and cytoskeletal elements to form macromolecular complexes at specialized subcellular domains [5,6]. These dynamic protein–protein interactions regulate CFTR channel function as well as its localization and processing within cells [7,8]. We have shown that CFTR, lysophosphatidic acid receptor 2 (LPA_2), and Na^+/H^+ exchanger regulatory factor-2 (NHERF2) form macromolecular complexes at the plasma membrane of gut epithelia, which functionally couple LPA_2 signaling to CFTR-mediated Cl^- transport [9]. LPA_2 is a G protein-coupled receptor that binds the lipid signaling molecule LPA and mediates diverse cellular responses such as cell proliferation and platelet aggregation [10]. NHERF2 is a PDZ domain-containing protein that typically functions as a scaffold to cluster transporters, receptors, and signaling molecules into supramolecular complexes [11]. We have demonstrated that LPA inhibits both CFTR-mediated Cl^- transport through the LPA_2-mediated Gi pathway in a compartmentalized manner in cells and CFTR-dependent cholera toxin-induced mouse intestinal-fluid secretion in vivo [9]. We also demonstrated that disruption of the PDZ-mediated NHERF2–LPA_2 interaction abolishes the LPA inhibitory effect and augments CFTR Cl^- channel activity in Calu-3 cells and also in fluid secretion from pig tracheal submucosal glands [12]. These findings imply that targeting the PDZ-mediated NHERF2–LPA_2 interaction could provide new strategies for therapeutic interventions of CFTR-associated diseases [8,12].

* Corresponding authors. Address: 540 E. Canfield Street, Detroit, Michigan 48201, USA. Fax: +1 313 577 2765 (Z. Yang). Address: 3333 Burnet Avenue, Cincinnati, OH 45229, USA (A.P. Naren).

E-mail addresses: zyang@med.wayne.edu (Z. Yang), anaren@cchmc.org (A.P. Naren).

http://dx.doi.org/10.1016/j.bbrc.2014.02.128
0006-291X/© 2014 Elsevier Inc. All rights reserved.

In general, PDZ domains mediate protein interactions by recognizing the C-terminal sequence of target proteins and binding to the targets through a canonically and structurally conserved PDZ peptide-binding pocket [13]. Based on the residues at positions 0 and −2 of the peptides (position 0 referring to the C-terminal residue), early studies have grouped PDZ domains into two major specificity classes: class I, (S/T)X(V/I/L) (X denoting any amino acid); class II, (F/Y)X(F/V/A) [14–16]. However, more recent mounting evidence indicates that PDZ specificity is unexpectedly complex and diverse, with the PDZ domain family recognizing up to seven C-terminal ligand residues and forming at least 16 unique specificity classes [17]. The complexity of PDZ-peptide interactions is further exemplified by the facts that many PDZ domains can bind to multiple ligands of different peptide classes and that single peptides are capable of binding to distinct PDZ domains [17]. This complex picture of PDZ-peptide interactions raises a challenging problem regarding how PDZ domains, structurally simple protein-interaction modules, achieve binding promiscuity and specificity concomitantly, the nature of which remains obscure. In this context, we present the crystal structure of NHERF2 PDZ1 in complex with the LPA_2 C-terminal peptide MDSTL. The structure reveals that the LPA_2 peptide binds to PDZ1 in an extended conformation with the last four residues making specific side chain contacts. Comparison of the PDZ1–LPA_2 structure to the structure of PDZ1 in complex with a different peptide suggests that the binding diversity of PDZ1 is facilitated by the conformational flexibility in the peptide-binding pocket. This study provides the structural basis of the PDZ-mediated NHERF2–LPA_2 interaction and could be valuable in the development of novel therapeutic strategies against CFTR-related human diseases.

2. Materials and methods

2.1. Protein expression and purification

A DNA fragment encoding the human NHERF2 PDZ1 (residues 9–90) was amplified by PCR using the full-length human NHERF2 cDNA as a template. The C-terminal extension MDSTL that corresponds to residues 347–351 of human LPA_2 was created by inclusion of 15 extra bases in the reverse primer. The PCR products were cloned in the pSUMO vector containing an N-terminal His6-SUMO tag. The resulting clone was transformed into *Escherichia coli* BL21 Condon Plus (DE3) cells for protein expression. The transformants were grown to an OD600 (optical density at 600 nm) of 0.4 at 37 °C in LB medium, and then induced with 0.1 mM isopropylthio-β-D-galactoside at 15 °C overnight. The cells were harvested by centrifugation and lysed by French Press. The soluble fraction was then subjected to Ni^{2+} affinity chromatography purification, followed by the cleavage of the His6-SUMO tag with yeast SUMO Protease 1. PDZ1 proteins were separated from the cleaved tag by a second Ni^{2+} affinity chromatography and further purified by size-exclusion chromatography. Finally, the proteins were concentrated to 20–30 mg/ml in a buffer containing 20 mM Tris–HCl (pH 8.0), 150 mM NaCl, 1 mM β-mercaptoethanol (BME), and 5% glycerol.

2.2. Crystallization, data collection and structure determination

Crystals were grown by the hanging-drop vapor-diffusion method by mixing the protein (~20 mg/ml) with an equal volume of a reservoir solution containing 100 mM HEPES, pH 7.0, 0.2 M potassium thiocyanate (KSCN), 25% PEG3350 at 20 °C. Crystals typically appeared overnight and continued to grow to their full size in 2–3 days. Prior to X-ray diffraction data collection, crystals were cryoprotected in a solution containing the mother liquor and 25% glycerol and flash cooled in liquid nitrogen. The data were collected at 100 K at beamline 21-ID-F at the Advanced Photon Source (Argonne, IL) and processed and scaled using the program XDS [18]. Crystals belong to the space group $P2_1$ with unit cell dimensions $a = 26.4$ Å, $b = 40.3$ Å, $c = 37.1$ Å, $\beta = 107.4°$, and one molecule in the asymmetric unit (Table 1). The structure was solved by the molecular replacement method with the program PHASER [19] using the PDZ1–EDTSV structure (PDB code: 2OCS) as a search model. Structure modeling was carried out in COOT [20], and refinement was performed with PHENIX [21]. To reduce the effects of model bias, iterative-build OMIT maps were used during model building and structure refinement. The final models were analyzed and validated with Molprobity [22]. All figures of 3D representations of the PDZ1–LPA_2 structure were made with PyMOL (www.pymol.org).

Table 1
Crystallographic data and refinement statistics.

Data	
Space group	$P2_1$
Cell parameters (Å)	
a	26.4
b	40.3
c	37.1
Wavelength (Å)	1.2719
Resolution (Å)	24.2–1.34 (1.37–1.34)
R_{merge} [a]	0.039 (0.250) [b]
Redundancy	4.1 (4.0)
Unique reflections	17,966
Completeness (%)	99.8 (99.6)
$\langle I/\sigma \rangle$	15.3 (3.0)
Refinement	
Resolution (Å)	24.2–1.34 (1.37–1.34)
Molecules/AU	1
R_{work} [c]	0.145 (0.268)
R_{free} [d]	0.177 (0.275)
Ramachandran plot	
Residues in favored	97.9%
Residues in allowed	2.1%
RMSD	
Bond lengths (Å)	0.007
Bond angels (°)	1.2
No. of atoms	
Protein	1347
Peptide	73
Water	143
Chloride	2
B-factor (Å^2)	
Protein	17.2
Peptide	17.7
Water	28.5
Chloride	20.2
SCN	12.4

[a] $R_{merge} = \Sigma|I - \langle I \rangle|/\Sigma I$, where I is the observed intensity and $\langle I \rangle$ is the averaged intensity of multiple observations of symmetry-related reflections.
[b] Numbers in parentheses refer to the highest resolution shell.
[c] $R_{work} = \Sigma|F_o - F_c|/\Sigma|F_o|$, where F_o is the observed structure factor, F_c is the calculated structure factor.
[d] R_{free} was calculated using a subset (5%) of the reflection not used in the refinement.

2.3. Protein data bank accession number

Coordinates and structure factors have been deposited in the Protein Data Bank with accession number 4P0C.

3. Results and discussion

3.1. Specificity determinants of NHERF2–LPA_2 interaction

The overall structure of NHERF2 PDZ1 is similar to other PDZ domains [16,23], consisting of six β strands (β1–β6) and two

α-helices (αA and αB) (Fig. 1A and B). The LPA_2 peptide binds in the cleft between β2 and αB, burying a total solvent-accessible surface area of 472 $Å^2$. The binding specificity of the PDZ1-LPA_2 interaction is achieved through networks of hydrogen bonds and hydrophobic interactions (Fig. 1C). At the ligand position 0, the side chain of Leu0 is nestled in a deep hydrophobic pocket formed by invariant residues Tyr21, Phe23, and Leu25 from β2 and Val73 and Ile76 from αB (Fig. 1D). In the pocket, the position of Leu0 is further secured by both a hydrogen bond from its amide nitrogen to the Phe23 carbonyl oxygen and triplet hydrogen bonding between the Leu0 carboxylate and the amides of Tyr21, Gly22, and Phe23. Similar interactions have been observed in several other PDZ-mediated complexes [16,23], which represent the most-conserved binding mode for terminal Leu recognition. Residues at other peptide positions also contribute to the PDZ1–LPA_2 complex formation (Fig. 1C). At position −1, the side chain hydroxyl of Thr-1 forms a hydrogen bond with the Nδ1 atom of the His24 imidazole ring. At position −2, Ser-2 makes one hydrogen bond to the His69 imidazole group and two hydrogen bonds to the highly conserved residue Leu25. At the ligand position -3, the interactions with Asp-3 include one hydrogen bond from its side chain carboxylate to the side chain of His24 and another hydrogen bond to the Nδ1 atom of His26. The latter interaction represents an unusual variation in this structure, since the negatively charged Asp-3 is generally recognized by an Arg residue at Arg37 position in other PDZ complexes [24]. Finally, the peptide residue Met-4 engages in a main-chain contact with Gly27, but does not participate in any specific side-chain interactions. These observations indicate that the last four residues of LPA_2 contribute to the binding specificity in the PDZ1–LPA_2 complex formation.

3.2. Structural basis of broad PDZ1 binding specificity

To gain further insights into PDZ1 binding specificity, we compared the PDZ1–LPA_2 structure to the structure of PDZ1 in complex with a different peptide (EDTSV) (Fig. 2). The overall structures of the two liganded PDZs are very similar, with a root mean square difference (RMSD) of 0.20 Å for 85 Cα atoms (Fig. 2A). The main chains of the bound peptides superimpose well (RMSD of 0.16 Å), as do their relative spatial positions to the conserved PDZ motifs. These observations indicate that binding of different peptides has little effect on the PDZ1 overall fold, consistent with previous evidence that the localized changes at a few key positions within HtrA1 PDZ are responsible for dramatically altered PDZ binding specificity [23]. Close examination of the structural alignment reveals some similarities, but also substantial differences, in the peptide-binding pockets (Fig. 2B). At the ligand position 0, the side chains of LPA_2 Leu0 and EDTSV Val0 follow a similar path entering a pocket that is virtually identical between the two PDZ1 structures. At the ligand position −2, recognition of Ser-2 and Thr-2 is achieved by similar mechanisms where there is a direct hydrogen bond to the side chain of the structurally conserved His69 in both cases. However, large differences are observed around the residues at the −1 position of the ligands (Fig. 2C). In PDZ1–LPA_2, His24 adopts a single conformation that simultaneously binds to Thr-1 and Asp-3. In PDZ1–EDTSV, His24 has a double conformation in which conformation 1 is similar to the one observed for PDZ1–LPA_2, but conformation 2 represents a new conformer with the side chain packing against the hydroxyl of Ser-1. This conformational change is accompanied by large alteration in the Arg38 rotameric states. In PDZ1–EDTSV, the side chain of Arg38 points away from the bound peptide, whereas in PDZ1–LPA_2 it adopts a double conformation with one conformation oriented toward the Thr-1 residue. These observed differences suggest that the conformational changes of His24 and Arg38 underlie the NHERF2 PDZ1 flexibility to accommodate ligands with different −1 side chains and denote a structural explanation for diverse peptide recognition.

3.3. Drug design perspective and novel SCN binding site

CFTR protein is the product of the *CFTR* gene mutated in patients with CF, which is a lethal autosomal-recessive genetic

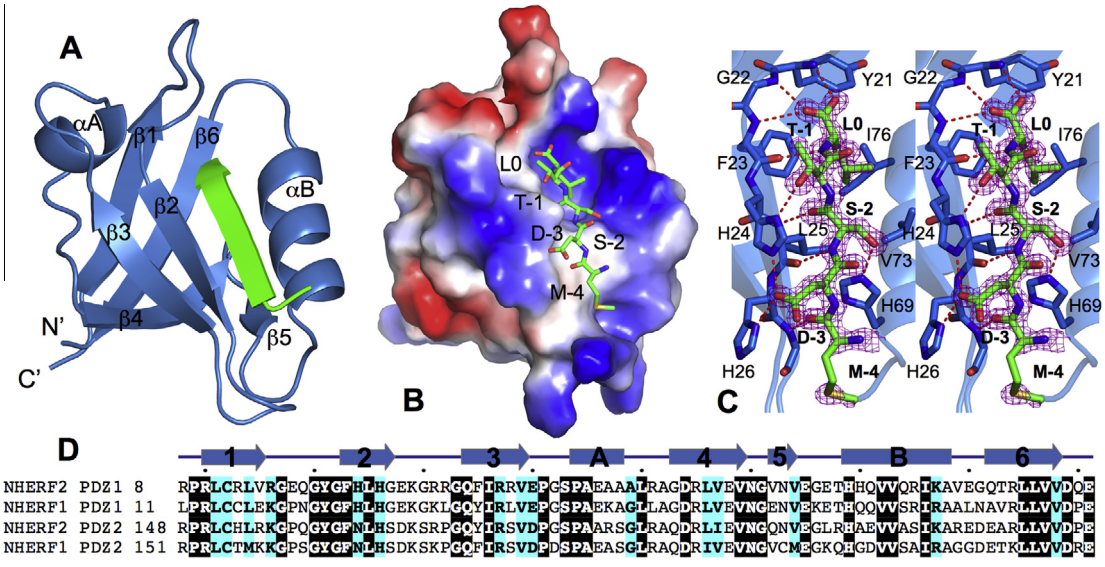

Fig. 1. Structure of NHERF2 PDZ1 in complex with the LPA_2 C-terminal sequence MDSTL. (A) Ribbon diagram of the PDZ1–LPA_2 structure. PDZ1 is shown in light blue and the LPA_2 peptide is shown in green. Secondary structures of PDZ1, α-helices, and β-strands are labeled and numbered according to their position in the sequence. (B) Surface representation of the PDZ1–LPA_2 structure. Surface coloring is according to the electrostatic potential: red, white, and blue correspond to negative, neutral, and positive potential, respectively. The vacuum electrostatics/protein contact potential was generated by PyMOL. The LPA_2 peptide is depicted by sticks. (C) Stereo view of the PDZ1 ligand-binding site bound to the LPA_2 C-terminal peptide. PDZ1 residues are represented by sticks with their carbon atoms colored in light blue. The LPA_2 peptide is depicted by sticks overlaid with $2F_o - F_c$ omit map calculated at 1.34 Å and contoured at 1.8 σ. Hydrogen bonds are illustrated as red broken lines. (D) Sequence alignment of selected PDZ domains. The alignment was performed by ClustalW [32], including human NHERF1 and NHERF2. Identical residues are shown as white on black, and similar residues appear shaded in cyan. Secondary structure elements are displayed above the sequences and labeled according to the scheme in Fig. 1A. Sequence numbering is displayed to the left of the sequences, with every 10th residue marked by a dot shown above the alignment. (For interpretation of the references to colour in this figure legend, the reader is referred to the web version of this article.)

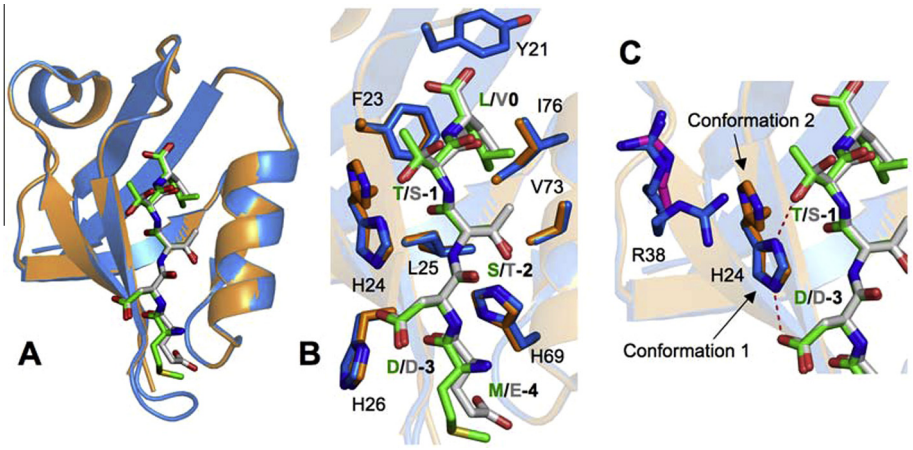

Fig. 2. Structural comparison of NHERF2 PDZ1 domains. (A) Superposition of the structures of PDZ1–LPA_2 (light blue; PDB code: 4P0C) and PDZ1-EDTSV (orange; PDB code: 2OCS). PDZ domains are represented by ribbons. Residues in the ligands are displayed as sticks. Carbon atoms are shown in green for LPA_2 and in gray for EDTSV. (B) Superposition of the PDZ1 ligand-binding pockets. Both PDZ1 and ligand residues are depicted by sticks and colored according to the scheme in Fig. 2A. (C) Close-up view of structural differences of His24 and Arg38. Red broken lines represent hydrogen bonds between His24 and LPA_2. (For interpretation of the references to colour in this figure legend, the reader is referred to the web version of this article.)

disease that is most common among Caucasians [25]. We previously have suggested that targeting the NHERF2–LPA_2 interaction may have a therapeutic potential in CF treatment, as inhibition of this interaction has been found to be sufficient to enhance CFTR channel activity both in vitro and in vivo [8,12]. These previous findings highlight the significance of our present structure studies and also imply that the structural details of the NHERF2–LPA_2 interaction may be valuable in developing new methods and strategies for selective drug design. For instance, this information can be used to create new NHERF2 inhibitors that are potent and specific to block the NHERF2–LPA_2 interaction. Such inhibitors have the potential to rescue epithelial cell function in the human CF airway by restoring or increasing CFTR channel activity. However, it should be noted that NHERF2 is capable of binding to a multitude of ligands, through which it regulates many cellular processes essential to normal physiological functions, such as testicular differentiation, signal transduction, endosomal recycling, membrane targeting, and hormone receptor desensitization [26–29]. It is therefore conceivable that the engagement of an inhibitor with the ligand-binding site would interfere with the full spectrum of NHERF2 PDZ-target interactions and could lead to considerable risks with a diverse range of unwanted physiological and hormonal abnormalities. In order to achieve NHERF2 inhibitor selectivity, one possible solution to this challenge is designing partially competitive inhibitors that only affect ligand-specific interactions and bind to a site other than the ligand-binding pocket. In this regard, it is interesting to note that the present structure reveals a small surface pocket adjacent to the ligand binding site (Fig. 3). This pocket is identified based on an extra electron density observed at the surface of the PDZ1 structure (Fig. 3A). Based on the components in the crystal condition and the shape of the density, the density was assigned as a thiocyanate molecule (SCN). Residues contributing to SCN binding include His26 from β2, Gly53 from β4, and Phe35 and Arg37 from β3 (Fig. 3B). Note that residues His26 and Arg37 shared by the ligand binding site and the SCN binding site are highly conserved (Fig. 1D), and these sites have been implicated in ligand-specific interactions in other PDZ domains [30,31]. Therefore, strategies aiming at exploiting the novel SCN binding site may represent a promising approach to achieve NHERF2-inhibitor selectivity that would allow the differentiation among a wide range of NHERF2-mediated interactions. Such strategy should have important implications in specific NHERF2 scaffolding regulation and also in many CFTR-dependent human diseases.

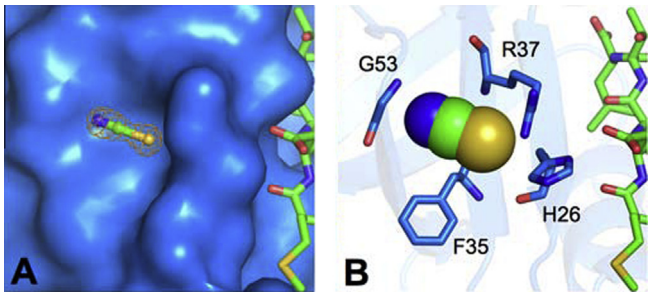

Fig. 3. SCN binding pocket. (A) Surface representation of the SCN binding site. PDZ1 surface is colored in light blue. LPA_2 residues are represented by sticks with their carbon atoms colored in green. SCN is depicted by balls-and-sticks overlaid with $2F_o - F_c$ omit map calculated at 1.34 Å and contoured at 1.8 σ. (B) Putative SCN-interacting residues. PDZ1 residues are shown in light blue and LPA_2 residues are shown in green. SCN is depicted by spheres. (For interpretation of the references to colour in this figure legend, the reader is referred to the web version of this article.)

Acknowledgments

This study was supported by the Leukemia Research Foundation, Aplastic Anemia & MDS International Foundation, and American Heart Association Grant Number 0835085N (to Z.Y.) and from the National Institutes of Health (DK-093045 and DK-080834 to A.P.N.). The authors are grateful to J. Denise Wetzel, CCHMC Medical Writer, for critical review of the manuscript.

References

[1] J.R. Riordan, J.M. Rommens, B. Kerem, N. Alon, R. Rozmahel, Z. Grzelczak, J. Zielenski, S. Lok, N. Plavsic, J.L. Chou, et al., Identification of the cystic fibrosis gene: cloning and characterization of complementary DNA, Science 245 (1989) 1066–1073.
[2] M.P. Anderson, R.J. Gregory, S. Thompson, D.W. Souza, S. Paul, R.C. Mulligan, A.E. Smith, M.J. Welsh, Demonstration that CFTR is a chloride channel by alteration of its anion selectivity, Science 253 (1991) 202–205.
[3] S.T. Ballard, D. Spadafora, Fluid secretion by submucosal glands of the tracheobronchial airways, Respir. Physiol. Neurobiol. 159 (2007) 271–277.
[4] J.R. Riordan, CFTR function and prospects for therapy, Annu. Rev. Biochem. 77 (2008) 701–726.
[5] C. Li, A.P. Naren, Macromolecular complexes of cystic fibrosis transmembrane conductance regulator and its interacting partners, Pharmacol. Ther. 108 (2005) 208–223.
[6] C. Li, A.P. Naren, CFTR chloride channel in the apical compartments: spatiotemporal coupling to its interacting partners, Integr. Biol. (Camb) 2 (2010) 161–177.

[7] A.P. Naren, B. Cobb, C. Li, K. Roy, D. Nelson, G.D. Heda, J. Liao, K.L. Kirk, E.J. Sorscher, J. Hanrahan, J.P. Clancy, A macromolecular complex of beta 2 adrenergic receptor, CFTR, and ezrin/radixin/moesin-binding phosphoprotein 50 is regulated by PKA, Proc. Natl. Acad. Sci. USA 100 (2003) 342–346.
[8] H. Penmatsa, W. Zhang, S. Yarlagadda, C. Li, V.G. Conoley, J. Yue, S.W. Bahouth, R.K. Buddington, G. Zhang, D.J. Nelson, M.D. Sonecha, V. Manganiello, J.J. Wine, A.P. Naren, Compartmentalized cyclic adenosine 3′,5′-monophosphate at the plasma membrane clusters PDE3A and cystic fibrosis transmembrane conductance regulator into microdomains, Mol. Biol. Cell 21 (2010) 1097–1110.
[9] C. Li, K.S. Dandridge, A. Di, K.L. Marrs, E.L. Harris, K. Roy, J.S. Jackson, N.V. Makarova, Y. Fujiwara, P.L. Farrar, D.J. Nelson, G.J. Tigyi, A.P. Naren, Lysophosphatidic acid inhibits cholera toxin-induced secretory diarrhea through CFTR-dependent protein interactions, J. Exp. Med. 202 (2005) 975–986.
[10] F.T. Lin, Y.J. Lai, Regulation of the LPA2 receptor signaling through the carboxyl-terminal tail-mediated protein-protein interactions, Biochim. Biophys. Acta 1781 (2008) 558–562.
[11] S. Shenolikar, E.J. Weinman, NHERF: targeting and trafficking membrane proteins, Am. J. Physiol. Renal Physiol. 280 (2001) F389–F395.
[12] W. Zhang, H. Penmatsa, A. Ren, C. Punchihewa, A. Lemoff, B. Yan, N. Fujii, A.P. Naren, Functional regulation of cystic fibrosis transmembrane conductance regulator-containing macromolecular complexes: a small-molecule inhibitor approach, Biochem. J. 435 (2011) 451–462.
[13] B.Z. Harris, W.A. Lim, Mechanism and role of PDZ domains in signaling complex assembly, J. Cell Sci. 114 (2001) 3219–3231.
[14] M. Sheng, C. Sala, PDZ domains and the organization of supramolecular complexes, Annu. Rev. Neurosci. 24 (2001) 1–29.
[15] H.J. Lee, J.J. Zheng, PDZ domains and their binding partners: structure, specificity, and modification, Cell Commun. Signal. 8 (2010) 8.
[16] S. Karthikeyan, T. Leung, J.A. Ladias, Structural basis of the Na+/H+ exchanger regulatory factor PDZ1 interaction with the carboxyl-terminal region of the cystic fibrosis transmembrane conductance regulator, J. Biol. Chem. 276 (2001) 19683–19686.
[17] R. Tonikian, Y. Zhang, S.L. Sazinsky, B. Currell, J.H. Yeh, B. Reva, H.A. Held, B.A. Appleton, M. Evangelista, Y. Wu, X. Xin, A.C. Chan, S. Seshagiri, L.A. Lasky, C. Sander, C. Boone, G.D. Bader, S.S. Sidhu, A specificity map for the PDZ domain family, PLoS Biol. 6 (2008) e239.
[18] W. Kabsch, Xds, Acta Crystallogr. D Biol. Crystallogr. 66 (2010) 125–132.
[19] A.J. McCoy, R.W. Grosse-Kunstleve, P.D. Adams, M.D. Winn, L.C. Storoni, R.J. Read, Phaser crystallographic software, J. Appl. Crystallogr. 40 (2007) 658–674.
[20] P. Emsley, K. Cowtan, Coot: model-building tools for molecular graphics, Acta Crystallogr. D Biol. Crystallogr. 60 (2004) 2126–2132.
[21] P.D. Adams, P.V. Afonine, G. Bunkoczi, V.B. Chen, I.W. Davis, N. Echols, J.J. Headd, L.W. Hung, G.J. Kapral, R.W. Grosse-Kunstleve, A.J. McCoy, N.W. Moriarty, R. Oeffner, R.J. Read, D.C. Richardson, J.S. Richardson, T.C. Terwilliger, P.H. Zwart, PHENIX: a comprehensive Python-based system for macromolecular structure solution, Acta Crystallogr. D Biol. Crystallogr. 66 (2010) 213–221.
[22] V.B. Chen, W.B. Arendall 3rd, J.J. Headd, D.A. Keedy, R.M. Immormino, G.J. Kapral, L.W. Murray, J.S. Richardson, D.C. Richardson, MolProbity: all-atom structure validation for macromolecular crystallography, Acta Crystallogr. D Biol. Crystallogr. 66 (2010) 12–21.
[23] S.T. Runyon, Y. Zhang, B.A. Appleton, S.L. Sazinsky, P. Wu, B. Pan, C. Wiesmann, N.J. Skelton, S.S. Sidhu, Structural and functional analysis of the PDZ domains of human HtrA1 and HtrA3, Protein Sci. 16 (2007) 2454–2471.
[24] S. Karthikeyan, T. Leung, J.A. Ladias, Structural determinants of the Na+/H+ exchanger regulatory factor interaction with the beta 2 adrenergic and platelet-derived growth factor receptors, J. Biol. Chem. 277 (2002) 18973–18978.
[25] W. Zhang, N. Fujii, A.P. Naren, Recent advances and new perspectives in targeting CFTR for therapy of cystic fibrosis and enterotoxin-induced secretory diarrheas, Future Med. Chem. 4 (2012) 329–345.
[26] L. Thevenet, K.H. Albrecht, S. Malki, P. Berta, B. Boizet-Bonhoure, F. Poulat, NHERF2/SIP-1 interacts with mouse SRY via a different mechanism than human SRY, J. Biol. Chem. 280 (2005) 38625–38630.
[27] Y.S. Oh, N.W. Jo, J.W. Choi, H.S. Kim, S.W. Seo, K.O. Kang, J.I. Hwang, K. Heo, S.H. Kim, Y.H. Kim, I.H. Kim, J.H. Kim, Y. Banno, S.H. Ryu, P.G. Suh, NHERF2 specifically interacts with LPA2 receptor and defines the specificity and efficiency of receptor-mediated phospholipase C-beta3 activation, Mol. Cell. Biol. 24 (2004) 5069–5079.
[28] P. He, S.J. Lee, S. Lin, U. Seidler, F. Lang, G. Fejes-Toth, A. Naray-Fejes-Toth, C.C. Yun, Serum- and glucocorticoid-induced kinase 3 in recycling endosomes mediates acute activation of Na+/H+ exchanger NHE3 by glucocorticoids, Mol. Biol. Cell 22 (2011) 3812–3825.
[29] R. Padanyi, Y. Xiong, G. Antalffy, K. Lor, K. Paszty, E.E. Strehler, A. Enyedi, Apical scaffolding protein NHERF2 modulates the localization of alternatively spliced plasma membrane Ca2+ pump 2B variants in polarized epithelial cells, J. Biol. Chem. 285 (2010) 31704–31712.
[30] G. Lu, Y. Wu, Y. Jiang, S. Wang, Y. Hou, X. Guan, J. Brunzelle, N. Sirinupong, S. Sheng, C. Li, Z. Yang, Structural insights into neutrophilic migration revealed by the crystal structure of the chemokine receptor CXCR2 in complex with the first PDZ domain of NHERF1, PLoS ONE 8 (2013) e76219.
[31] Y. Jiang, G. Lu, L.R. Trescott, Y. Hou, X. Guan, S. Wang, A. Stamenkovich, J. Brunzelle, N. Sirinupong, C. Li, Z. Yang, New conformational state of NHERF1–CXCR2 signaling complex captured by crystal lattice trapping, PLoS ONE 8 (2013) e81904.
[32] M.A. Larkin, G. Blackshields, N.P. Brown, R. Chenna, P.A. McGettigan, H. McWilliam, F. Valentin, I.M. Wallace, A. Wilm, R. Lopez, J.D. Thompson, T.J. Gibson, D.G. Higgins, Clustal W and Clustal X version 2.0, Bioinformatics 23 (2007) 2947–2948.